Editors' Suggestion | Featured in Physics

Photonic Anomalous Quantum Hall Effect

Sunil Mittal,[1,2,*] Venkata Vikram Orre,[1,2] Daniel Leykam,[3] Y. D. Chong,[4,5] and Mohammad Hafezi[1,2,6]
[1]Joint Quantum Institute, NIST/University of Maryland, College Park, Maryland 20742, USA
[2]Department of Electrical and Computer Engineering, and IREAP, University of Maryland, College Park, Maryland 20742, USA
[3]Center for Theoretical Physics of Complex Systems, Institute for Basic Science (IBS), Daejeon 34126, Republic of Korea
[4]Division of Physics and Applied Physics, School of Physical and Mathematical Sciences, Nanyang Technological University, Singapore 637371, Singapore
[5]Centre for Disruptive Photonic Technologies, Nanyang Technological University, Singapore 637371, Singapore
[6]Department of Physics, University of Maryland, College Park, Maryland 20742, USA

(Received 1 April 2019; published 23 July 2019)

We experimentally realize a photonic analogue of the anomalous quantum Hall insulator using a two-dimensional (2D) array of coupled ring resonators. Similar to the Haldane model, our 2D array is translation invariant, has a zero net gauge flux threading the lattice, and exploits next-nearest neighbor couplings to achieve a topologically nontrivial band gap. Using direct imaging and on-chip transmission measurements, we show that the band gap hosts topologically robust edge states. We demonstrate a topological phase transition to a conventional insulator by frequency detuning the ring resonators and thereby breaking the inversion symmetry of the lattice. Furthermore, the clockwise or the counterclockwise circulation of photons in the ring resonators constitutes a pseudospin degree of freedom. The two pseudospins acquire opposite hopping phases, and their respective edge states propagate in opposite directions. These results are promising for the development of robust reconfigurable integrated nanophotonic devices for applications in classical and quantum information processing.

DOI: 10.1103/PhysRevLett.123.043201

Photonics has emerged as a versatile platform to explore model systems with nontrivial band topology, a phenomenon originally associated with condensed matter systems [1–3]. Photonic systems have realized analogues of the integer quantum Hall effect [4–8], Floquet topological insulators [9–12], quantum spin-Hall and valley-Hall phases [13–18], and topological crystalline insulators [19,20]. Topological protection has enabled the realization of photonic devices that are robust against disorder, such as optical delay lines [7,8], lasers [21–23], and quantum light sources [24]. Moreover, features unique to bosonic systems, such as the possibility of introducing gain and loss [25–29], parametric driving, and squeezing of light [24,30,31], provide opportunities to explore topological phases that do not occur in fermionic systems.

Despite these advances, there has not yet been a nanophotonic realization of the anomalous quantum Hall phase—a two-dimensional Chern insulator with zero net gauge flux [32,33]. This is noteworthy since the various topological phases differ significantly in the realization of nontrivial band topology, offer different forms of topological protection, and are suited for different platforms. For instance, photonic spin-Hall phases based on degenerate orthogonal field polarizations have been realized at microwave frequencies [14,34], but have proven to be challenging to implement at optical frequencies using nanophotonic components. Photonic valley-Hall and topological crystalline phases, which rely on lattice symmetries, are easily realized at most frequencies including the optical regime [15,17,18,20,35], but their topological edge states manifest on internal boundaries instead of external edges [15,18–20,35] and are protected only against certain boundary deformations (e.g., 120° bends but not 90° bends) [15,19]. Quantum Hall and anomalous quantum Hall phases do not require any special symmetries and are therefore significantly more robust that other topological phases: topological edge states can appear along external edges and are protected irrespective of the lattice shape. The quantum Hall phase, which requires nonzero net gauge flux, has been realized in nanophotonics [6–8], but not the anomalous quantum Hall phase, which occurs in periodic lattices with zero net flux. Anomalous Hall lattices are highly advantageous for nanophotonic device applications, because their translational invariance allows for simpler structure designs and topological-to-trivial phase transitions can be easily induced by tuning on-site potentials [32].

In this work, we demonstrate a nanophotonic analogue of the anomalous quantum Hall system using a periodic 2D checkerboard lattice of coupled ring resonators specifically tailored to have strong next-nearest neighbor couplings [36]. The structure is implemented on a silicon-on-insulator platform and operates at telecom frequencies [7,8,37], with ring diameters and lattice periodicity on the order of

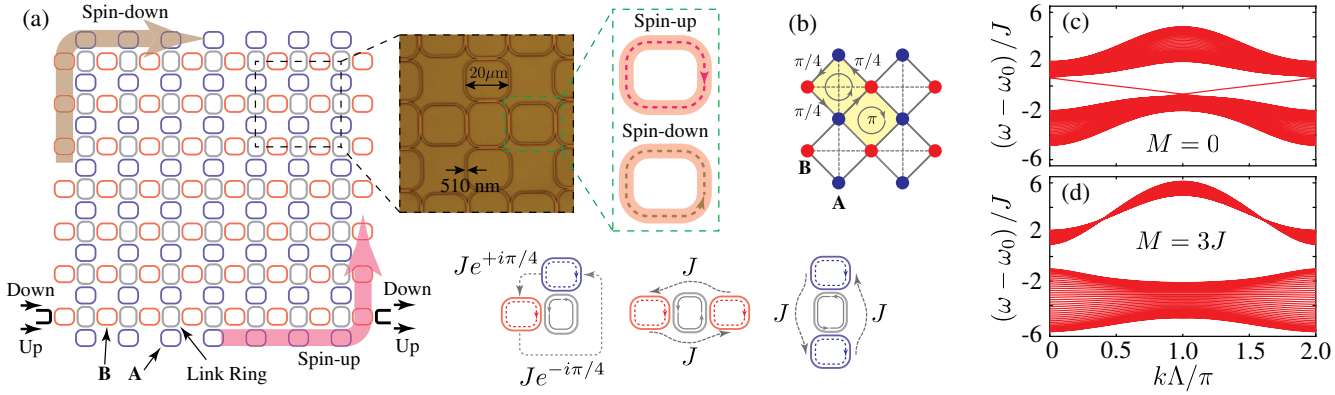

FIG. 1. (a) Schematic of the 2D array of ring resonators, with site rings **A** and **B** (blue and red, respectively) coupled using link rings (gray). The input and the output waveguides are shown in black. Top-left inset: Microscope image of the device. Top-right inset: The ring resonators support two pseudospins, up and down, which can be selectively excited and measured, and their corresponding edge states travel in opposite directions (pink and brown arrows, respectively). Bottom inset: Schematics for nearest-neighbor (left) and next-nearest-neighbor hoppings (center and right) for the pseudospin-up. (b) The effective 2D lattice. Solid (dashed) lines denote nearest (next-nearest)-neighbor hoppings, with hopping phases indicated. The gauge flux is $\pm\pi$ in a single plaquette, and zero over a unit cell of 2 plaquettes (shaded yellow). (c)–(d) Band diagram of a cylindrical lattice, for $M = 0$ and $M = 3J$, respectively. Here $k\Lambda$ is the phase between neighboring unit cells along the radial (periodic) direction. For $M < 2J$, the lattice is topological and exhibits edge states. The lattice is topologically trivial when $M > 2J$.

$20-50$ μm. As proposed in Ref. [38], the tight-binding description of the photonic lattice is similar to the Haldane model [32], in that the net gauge flux threading the lattice is zero, but next-nearest neighbor couplings induce nonzero local gauge flux. This effectively breaks time reversal symmetry and creates a topologically nontrivial band gap. We directly image the light intensity distribution in the lattice, revealing topological edge states in the gap that are robust against missing-site defects and can propagate around 90° corners without scattering into the bulk. As the overall structure is time-reversal invariant, it hosts a pseudospin degree of freedom associated with the clockwise and the counterclockwise (time-reversed) propagation of photons in the rings. By selective excitation of the pseudospins, we show that time-reversal invariance is effectively broken within each decoupled pseudospin sector, and the edge states associated with the two pseudospins propagate in opposite directions. Furthermore, we demonstrate a transition between topologically nontrivial and trivial phases by detuning the ring resonance frequencies, and observe edge states at an internal boundary between the two phases. Notably, the system is periodic and does not require staggering the phases of the couplings, unlike the coupled-resonator system of Refs. [6,7,23], which realizes the integer quantum Hall effect. These features are highly promising for topological nanophotonic devices that can be dynamically reconfigured via optical, electrical, or thermal pumping [38,39].

Our system, shown in Fig. 1(a), consists of two interposed square lattices of ring resonators, with respective sites labeled **A** and **B** [38]. These site-ring resonators are coupled to their neighbors and also next-nearest neighbors using another set of rings, the link rings. The resonance frequencies of the link rings are detuned from those of the site rings by one-half free-spectral range by introducing an extra path length such that the round-trip phase at site-ring frequencies is π [6,7]. The link rings thus introduce a direction-dependent hopping phase $\pm\pi/4$ from each lattice site to their nearest neighbors, while the hopping phase for next-nearest neighbors is zero [Fig. 1(a)]. As a result, the local effective magnetic flux (gauge flux) threading a plaquette of two **A** and two **B** site rings is $\pm\pi$, whereas the net flux threading a unit cell of two plaquettes is zero [Fig. 1(b)]. This staggered flux arrangement, originally conceived by Haldane, effectively breaks time-reversal symmetry and gives rise to an anomalous quantum Hall phase without Landau levels [32].

The photonic lattice is time-reversal invariant, and supports a pseudospin (up or down) degree of freedom associated with the circulation direction (clockwise or counterclockwise) of photons in the site-ring resonators [Fig. 1(a)]. The two pseudospins are time-reversed partners, and thus have identical coupling constants and resonance frequencies. However, they acquire opposite hopping phases between nearest neighbors, such that each pseudospin effectively experiences broken time-reversal symmetry and realizes a copy of the anomalous Hall phase [33] with the tight-binding Hamiltonian [38]

$$H=\sum_{i,\sigma}(\omega_0-M)a^\dagger_{i,\sigma}a_{i,\sigma}+(\omega_0+M)b^\dagger_{i,\sigma}b_{i,\sigma} - \sum_{\langle i,j\rangle,\sigma}J(a^\dagger_{j,\sigma}a_{i,\sigma}+b^\dagger_{j,\sigma}b_{i,\sigma}+a^\dagger_{j,\sigma}b_{i,\sigma}e^{-i\sigma\phi_{i,j}}+\text{H.c.}). \quad (1)$$

Here, $a_{i,\sigma}$, $b_{i,\sigma}$ are the annihilation operators corresponding to site rings **A** and **B**, respectively, at lattice site index

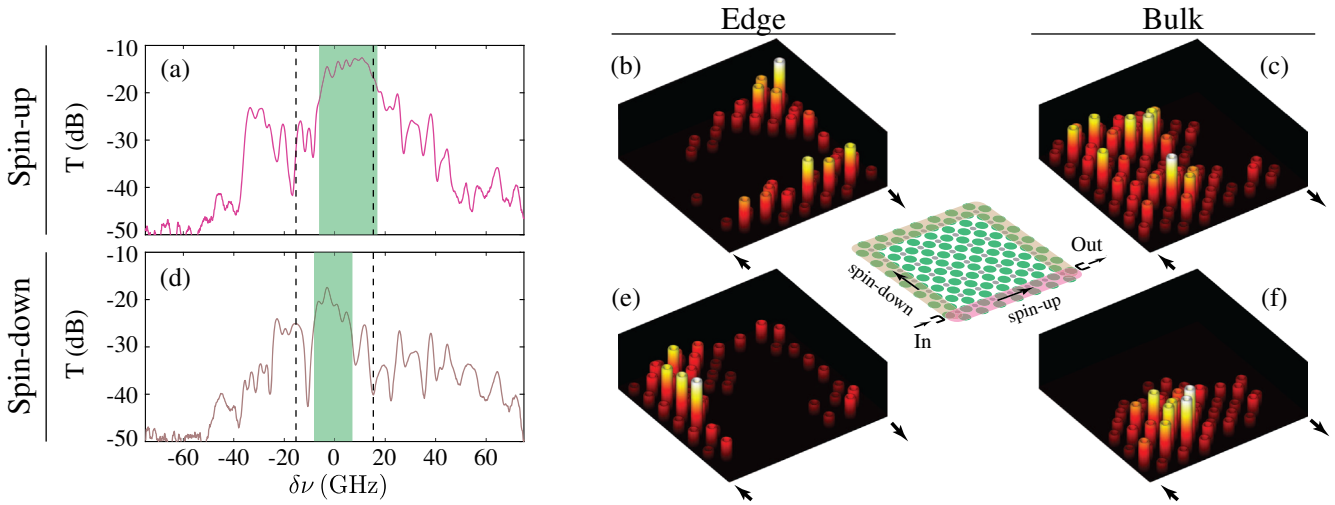

FIG. 2. (a) Measured transmission (T) spectrum for the topologically nontrivial lattice ($M = 0$) with the pseudospin-up excitation. The green shaded region indicates the frequency band over which topological edge states are observed in direct imaging and the dashed lines indicate the expected edge-band region for a pure device. (b) The corresponding spatial intensity distribution obtained through direct imaging at $\delta\nu \approx 0$ (integrated over a frequency range of 5 GHz). Edge states circulate CCW around the lattice. (c) Intensity distribution at $\delta\nu \approx -20$ GHz, showing scattering into the bulk. (d)–(f) The corresponding results for the pseudospin-down excitation. The edge states now circulate CW around the lattice. All spatial intensity distributions show only site ring resonators. The arrows indicate input and output ports for transmission measurements.

$i = (x, y)$ and the summation $\langle i, j \rangle$ is only over the nearest and next-nearest neighbors indicated in Fig. 1(b). $\sigma = \pm 1$ is the pseudospin index for the up or down spins, respectively. J is the coupling strength between the nearest and the next-nearest neighbor sites and $\phi = \pi/4$ is the direction-dependent hopping phase between sites **A** and **B**, as shown in Fig. 1(a). We include a frequency detuning M between the **A** and **B** site rings. When $M < 2J$, the lattice band structure hosts a topological band gap, occupied by unidirectional, topologically robust edge states [Fig. 1(c)] and their number constitutes a topological invariant [37,40]. When $M > 2J$, the lattice is topologically trivial and the edge states are absent [Fig. 1(d)]. Because of the spin-dependent hopping phase, the edge states corresponding to the two pseudospins propagate around the lattice in opposite directions, similar to the quantum spin-Hall effect [33]. Although the pseudospins do not follow Kramers degeneracy theorem and the edge states are therefore not robust against interspin coupling disorder, the mixing between pseudospins is negligible in the present system [7,8].

We implemented the design using silicon ring resonators with waveguides 510 nm wide, 220 nm high, and resonator length ≈70 μm. The gap between resonators is 180 nm, with coupling strength J estimated at 15.6(4) GHz (see Supplemental Material [41]). To probe the lattice, we couple a tunable continuous-wave laser at the input port and measure the power transmission at the output port [Fig. 1(b)]. By choosing the input and the output ports, we can selectively excite and measure a given pseudospin. A microscope objective is also used to directly image the spatial light intensity distribution [7].

To observe topological edge states, we fabricated an array of 56 **A** resonators and 56 **B** resonators, as shown schematically in Fig. 1(a). For this device we choose $M = 0$, that is, the **A** and **B** resonators are identical, corresponding to the nontrivial topological phase. Figure 2(a) shows the measured transmission spectrum at the lattice output for the pseudospin-up excitation. We observe high transmission near the frequency detuning $\delta\nu \approx 0$. Figure 2(b) shows the measured spatial intensity profile at $\delta\nu \approx 0$, integrated over a frequency range of 5 GHz. The light is confined to the lattice edge and propagates around the lattice in a counterclockwise direction. Furthermore, the light travels around two sharp 90° bends without scattering into the bulk of the lattice. This shows that this high-transmission region around $\delta\nu \approx 0$ is indeed the topological edge band. The decrease in light intensity as it propagates along the edge is mainly due to scattering losses in the resonator waveguides. By contrast, when we excite the lattice outside this band, e.g., at $\delta\nu \approx -20$ GHz, the spatial intensity distribution occupies the bulk of the lattice, as shown in Fig. 2(c). Moreover, the spatial intensity profile in the bulk band is sensitive to even small changes in the excitation frequency whereas the intensity profile in the edge band is relatively constant throughout the edge band. Note that the circulation direction (CCW) around the lattice is opposite to the circulation direction (CW) in the site ring resonators.

This observation of topological edge states is also a demonstration of their robustness against fabrication-induced disorder. Although the fabrication was performed at a state-of-the-art commercial foundry (IMEC, Belgium),

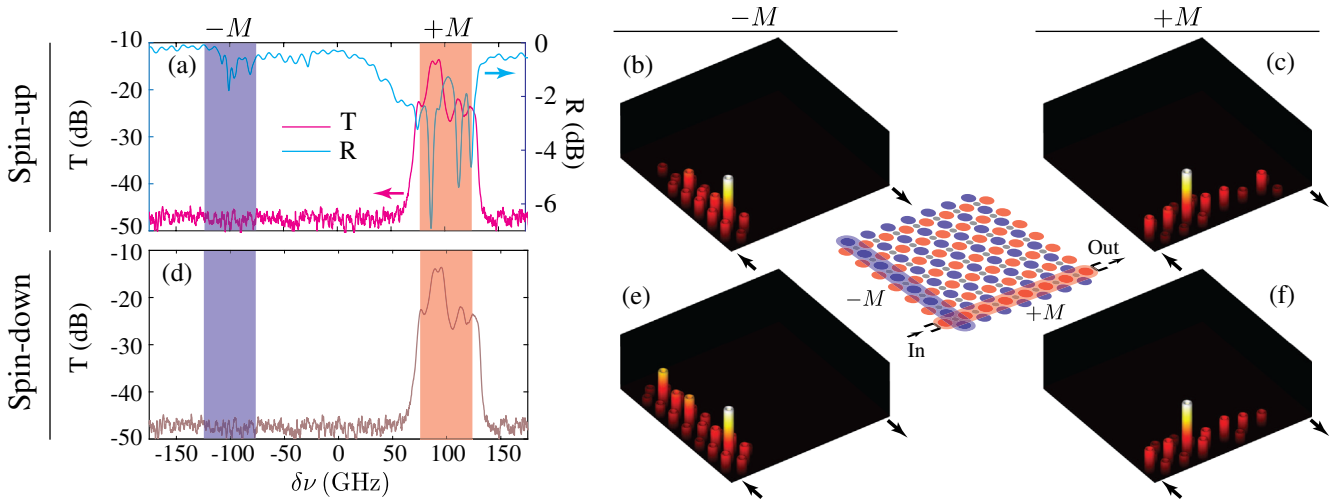

FIG. 3. (a) Measured transmission (T) and reflection (R) spectrum of a topologically trivial device, with $M \approx 98$ GHz $\gg 2J$ and pseudospin-up excitation. The transmission is negligible within the band gap ($\delta\nu \approx 0$) due to the absence of edge states. The transmission peak (and reflection dip) at $\delta\nu = +M$ coincides with the resonance frequency of the **B** rings. At $\delta\nu = -M$, the lattice absorbs some light from the input but the light does not reach the output because of the large frequency mismatch between the **A** and **B** rings. (b),(c) Spatial intensity profiles for $\delta\nu = +M$ and $\delta\nu = -M$, showing excitation of only the **B** and **A** rings, respectively. (d) Measured transmission spectrum for the pseudospin-down excitation. Unlike the topological case, the transmission is the same irrespective of the spin. (e),(f) Spatial intensity distributions also remain almost identical, confirming the topologically trivial nature of the lattice.

there is significant disorder in the ring resonance frequencies, which we measured to be around 33 GHz, comparable to the band gap width of $2J \approx 32$ GHz. Nevertheless, disorder decreases the width of the topological band gap and hence increases the transverse localization length of the edge states (see Supplemental Material [41]).

Next, we probe the spin-polarized nature of the topological edge states by exciting the lattice with the pseudospin-down. Figure 2(d) shows the resulting transmission spectrum. The measured spatial intensity profile at $\delta\nu \approx 0$ reveals an edge state that now propagates around the lattice in a clockwise direction [Fig. 2(e)]. Again, the edge state intensity is confined to the physical edge of the lattice. The transmission at $\delta\nu \approx 0$ is approximately 5 dB lower than in the pseudospin-up case, because the edge state for the pseudospin-down travels a much longer path between the input and output couplers. At frequencies outside the band gap, we again see scattering into the bulk [Fig. 2(f)]. Because of the disorder, the edge-band regions of the two pseudospins are slightly shifted in frequency.

To demonstrate the existence of a topological phase transition, we fabricated another device with sublattice detuning $M \approx 98$ GHz, significantly larger than the transition threshold of $2J \approx 31$ GHz. This detuning is achieved by increasing (decreasing) the length of the **A** (**B**) ring resonators by 30 nm, which red (blue) shifts their resonance frequencies. Figure 3(a) shows the measured transmission spectrum at the output, for the pseudospin-up input. We observe almost negligible transmission at $\delta\nu = 0$, indicating the absence of any transmitting channels in the band gap. There is a single transmission band at $\delta\nu \approx M \approx 100$ GHz. The measured spatial intensity distribution at $\delta\nu = 100$ GHz [Fig. 3(c)] reveals only a few **B** rings (which are resonant with the input frequency) are excited near the input port. In this regime, the **A** and **B** rings are very weakly coupled due to the large resonance frequency mismatch. The transmission is negligible at $\delta\nu = -100$ GHz (the resonance frequency of the **A** rings) because the input and output ports are coupled to **B** rings. A small amount of absorption by the **A** rings is visible in the reflection spectra shown in Fig. 3(a), and in the spatial intensity profile of Fig. 3(b). More importantly, we find that flipping the spin of excitation does not affect the transmission spectrum or the spatial intensity profile, as shown in Figs. 3(d)–3(f); this confirms the lattice is topologically trivial.

To verify that the edge states are not artifacts of the physical lattice boundary, we fabricated a device with an interface between a topological lattice ($M = 0$) and a trivial lattice ($M \approx 98$ GHz), shown in Fig. 4(a). We place an input port on one edge of the topologically nontrivial domain and monitor two output ports on the edges of the nontrivial and trivial domains. The measured transmission spectra at the two output ports, with the pseudospin-down excitation, are shown in Fig. 4(b). At frequencies within the band gap of the nontrivial domain [highlighted in Fig. 4(b)], we observe edge states propagating clockwise around the nontrivial domain [Fig. 4(c)]. These edge states then follow the "internal" domain boundary, and do not enter the topologically trivial domain; accordingly, negligible transmission is observed at the output port in the

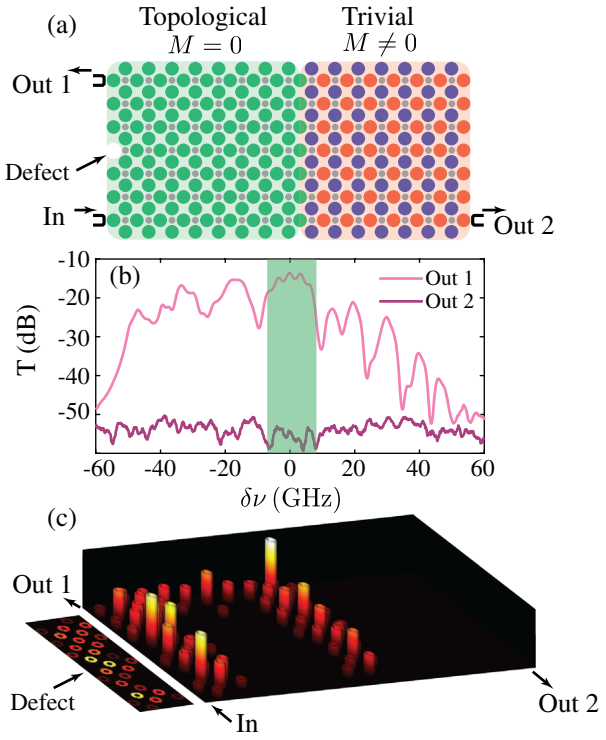

FIG. 4. (a) Schematic of device with an interface between topological ($M = 0$) and trivial ($M > 2J$) domains. The topological domain also hosts a defect in the form of a missing site-ring resonator. (b) Measured transmission (T) spectrum from input to the two output ports, for the pseudospin-down excitation. The light follows the interface, leading to negligible output at the trivial domain coupler. (c) Measured spatial intensity profile. The inset shows a 2D plot of the intensity distribution along the left edge with the defect.

trivial domain. As a further test of robustness, we deliberately removed one site-ring resonator from the edge of the topologically nontrivial domain, as indicated in Figs. 4(a) and 4(c). The edge state routes around the defect, without scattering into the bulk. We emphasize that this topological protection is superior to recently demonstrated crystalline symmetry-protected and valley-Hall topological edge states, which are sensitive to symmetry-breaking disorder [17,18,20,42,43].

To summarize, we demonstrated topologically robust edge states in a nanophotonic analogue of the anomalous quantum Hall effect, using a periodic 2D lattice of ring resonators with zero net gauge flux. We showed a topological-to-trivial phase transition, induced by relatively small detunings of the ring resonance frequencies. In the future, this phase transition can be utilized for robust routing and switching of light in integrated photonic devices [38]. Specifically, the silicon photonics platform can easily include active components, such as metal heaters [37] or electro-optic modulators [44] to dynamically tune the ring resonances. Moreover, the large Kerr nonlinearity of silicon could be leveraged for robust, optically reconfigurable light routing, and to explore the behavior of topological states in a nonlinear regime. Our design can also be implemented using other material platforms, such as silicon nitride, aluminum nitride, etc., to work near the visible wavelength region.

This research was supported by the AFOSR-MURI Grant No. FA9550-16-1-0323, the Physics Frontier Center at the Joint Quantum Institute, the Institute for Basic Science in Korea (IBS-R024-Y1), the Singapore MOE Academic Research Fund Tier 2 Grant No. MOE2015-T2-2-008, and the Singapore MOE Academic Research Fund Tier 3 Grant No. MOE2016-T3-1-006.

*mittals@umd.edu

[1] F. D. M. Haldane and S. Raghu, Phys. Rev. Lett. **100**, 013904 (2008).
[2] L. Lu, J. D. Joannopoulos, and M. Soljačić, Nat. Photonics **8**, 821 (2014).
[3] T. Ozawa, H. M. Price, A. Amo, N. Goldman, M. Hafezi, L. Lu, M. C. Rechtsman, D. Schuster, J. Simon, O. Zilberberg *et al.*, Rev. Mod. Phys. **91**, 015006 (2019).
[4] S. Raghu and F. D. M. Haldane, Phys. Rev. A **78**, 033834 (2008).
[5] Z. Wang, Y. Chong, J. D. Joannopoulos, and M. Soljačić, Nature (London) **461**, 772 (2009).
[6] M. Hafezi, E. A. Demler, M. D. Lukin, and J. M. Taylor, Nat. Phys. **7**, 907 (2011).
[7] M. Hafezi, S. Mittal, J. Fan, A. Migdall, and J. M. Taylor, Nat. Photonics **7**, 1001 (2013).
[8] S. Mittal, J. Fan, S. Faez, A. Migdall, J. M. Taylor, and M. Hafezi, Phys. Rev. Lett. **113**, 087403 (2014).
[9] M. C. Rechtsman, J. M. Zeuner, Y. Plotnik, Y. Lumer, D. Podolsky, F. Dreisow, S. Nolte, M. Segev, and A. Szameit, Nature (London) **496**, 196 (2013).
[10] M. Minkov and V. Savona, Optica **3**, 200 (2016).
[11] L. J. Maczewsky, J. M. Zeuner, S. Nolte, and A. Szameit, Nat. Commun. **8**, 13756 (2017).
[12] S. Mukherjee, A. Spracklen, M. Valiente, E. Andersson, P. Ohberg, N. Goldman, and R. R. Thomson, Nat. Commun. **8**, 13918 (2017).
[13] A. B. Khanikaev, S. H. Mousavi, W.-K. Tse, M. Kargarian, A. H. MacDonald, and G. Shvets, Nat. Mater. **12**, 233 (2013).
[14] X. Cheng, C. Jouvaud, X. Ni, S. H. Mousavi, A. Z. Genack, and A. B. Khanikaev, Nat. Mater. **15**, 542 (2016).
[15] T. Ma and G. Shvets, New J. Phys. **18**, 025012 (2016).
[16] F. Gao, H. Xue, Z. Yang, K. Lai, Y. Yu, X. Lin, Y. Chong, G. Shvets, and B. Zhang, Nat. Phys. **14**, 140 (2018).
[17] J. Noh, S. Huang, K. P. Chen, and M. C. Rechtsman, Phys. Rev. Lett. **120**, 063902 (2018).
[18] M. I. Shalaev, W. Walasik, A. Tsukernik, Y. Xu, and N. M. Litchinitser, Nat. Nanotechnol. **14**, 31 (2019).
[19] L.-H. Wu and X. Hu, Phys. Rev. Lett. **114**, 223901 (2015).
[20] S. Barik, A. Karasahin, C. Flower, T. Cai, H. Miyake, W. DeGottardi, M. Hafezi, and E. Waks, Science **359**, 666 (2018).

[21] P. St-Jean, V. Goblot, E. Galopin, A. Lemaître, T. Ozawa, L. Le Gratiet, I. Sagnes, J. Bloch, and A. Amo, Nat. Photonics **11**, 651 (2017).
[22] B. Bahari, A. Ndao, F. Vallini, A. El Amili, Y. Fainman, and B. Kanté, Science **358**, 636 (2017).
[23] M. A. Bandres, S. Wittek, G. Harari, M. Parto, J. Ren, M. Segev, D. N. Christodoulides, and M. Khajavikhan, Science **359**, eaar4005 (2018).
[24] S. Mittal, E. A. Goldschmidt, and M. Hafezi, Nature (London) **561**, 502 (2018).
[25] M. S. Rudner and L. S. Levitov, Phys. Rev. Lett. **102**, 065703 (2009).
[26] J. M. Zeuner, M. C. Rechtsman, Y. Plotnik, Y. Lumer, S. Nolte, M. S. Rudner, M. Segev, and A. Szameit, Phys. Rev. Lett. **115**, 040402 (2015).
[27] D. Leykam, K. Y. Bliokh, C. Huang, Y. D. Chong, and F. Nori, Phys. Rev. Lett. **118**, 040401 (2017).
[28] S. Yao and Z. Wang, Phys. Rev. Lett. **121**, 086803 (2018).
[29] Z. Gong, Y. Ashida, K. Kawabata, K. Takasan, S. Higashikawa, and M. Ueda, Phys. Rev. X **8**, 031079 (2018).
[30] V. Peano, M. Houde, F. Marquardt, and A. A. Clerk, Phys. Rev. X **6**, 041026 (2016).
[31] T. Shi, H. J. Kimble, and J. I. Cirac, Proc. Natl. Acad. Sci. U.S.A. **114**, E8967 (2017).
[32] F. D. M. Haldane, Phys. Rev. Lett. **61**, 2015 (1988).
[33] C. L. Kane and E. J. Mele, Phys. Rev. Lett. **95**, 226801 (2005).
[34] W.-J. Chen, S.-J. Jiang, X.-D. Chen, B. Zhu, L. Zhou, J.-W. Dong, and C. T. Chan, Nat. Commun. **5**, 5782 (2014).
[35] Y. Yang, Y. F. Xu, T. Xu, H.-X. Wang, J.-H. Jiang, X. Hu, and Z. H. Hang, Phys. Rev. Lett. **120**, 217401 (2018).
[36] A. W. W. Ludwig, M. P. A. Fisher, R. Shankar, and G. Grinstein, Phys. Rev. B **50**, 7526 (1994).
[37] S. Mittal, S. Ganeshan, J. Fan, A. Vaezi, and M. Hafezi, Nat. Photonics **10**, 180 (2016).
[38] D. Leykam, S. Mittal, M. Hafezi, and Y. D. Chong, Phys. Rev. Lett. **121**, 023901 (2018).
[39] M. I. Shalaev, S. Desnavi, W. Walasik, and N. M. Litchinitser, New J. Phys. **20**, 023040 (2018).
[40] W. Hu, J. C. Pillay, K. Wu, M. Pasek, P. P. Shum, and Y. D. Chong, Phys. Rev. X **5**, 011012 (2015).
[41] See Supplemental Material at http://link.aps.org/supplemental/10.1103/PhysRevLett.123.043201 for details of the experimental setup, disorder characterization, and transverse localization of the edge states.
[42] M. A. Gorlach, X. Ni, D. A. Smirnova, D. Korobkin, D. Zhirihin, A. P. Slobozhanyuk, P. A. Belov, A. Alu, and A. B. Khanikaev, Nat. Commun. **9**, 909 (2018).
[43] X.-T. He, E.-T. Liang, J.-J. Yuan, H.-Y. Qiu, X.-D. Chen, F.-L. Zhao, and J.-W. Dong, Nat. Commun. **10**, 872 (2019).
[44] G. T. Reed, G. Mashanovich, F. Y. Gardes, and D. J. Thomson, Nat. Photonics **4**, 518 (2010).